Boundary-Layer Meteorol
DOI 10.1007/s10546-011-9653-x

ARTICLE

The Height Correction of Similarity Functions in the Stable Boundary Layer

Zbigniew Sorbjan

Received: 5 January 2011 / Accepted: 11 August 2011
© The Author(s) 2011. This article is published with open access at Springerlink.com

Abstract Empirical similarity functions of the Richardson number, obtained from bin-averaged data in the lower part of the stable boundary layer, show an undesired dependence on height at which the observations are collected. A correction of this flaw is proposed and tested by employing the neutral mixing length l_o as a similarity scale for height. The function of height describing l_o is assumed to be linear in the surface layer, and approaching a specified value with increasing height. The modification does not alter the dependence of similarity functions on the Richardson number, and is shown to be supported by the Cooperative Atmospheric-Surface Exchange Study-1999 (CASES-99) data.

Keywords CASES-99 · Flux-based scaling · Gradient-based scaling · Similarity theory · Stable boundary layer

1 Introduction

The Monin–Obukhov theory (1954) is regarded as the major tool for understanding and describing near-surface turbulence. Its framework has been frequently applied during the past few decades to analyze numerous field observations. Data accumulated during recent years indicate, however, that the approach has intrinsic limitations in stable conditions. Specifically, the Monin–Obukhov similarity scales, u_*, T_*, decrease with thermal stability, while their relative errors increase, causing the values of the stability parameter, $L_* \sim u_*^2/T_*$, to be highly scattered. In addition, the dimensionless similarity functions and their argument z/L_*, contain common divisors (i.e., u_*, T_*), a property referred to as "self-correlation" (e.g., Baas et al. 2006). As a result, it is difficult to establish the form of empirical similarity functions with satisfactory confidence in very stable conditions.

Z. Sorbjan (✉)
Department of Physics, Marquette University, Milwaukee, WI 53201-1881, USA
e-mail: zbigniew.sorbjan@mu.edu

Z. Sorbjan
Institute of Geophysics, Polish Academy of Sciences, Warsaw, Poland

Published online: 06 September 2011

The described flaws can be remedied by defining similarity scales and similarity functions in terms of the gradients of scalars. The resulting similarity formulation avoids the singularity imposed by small values of scales, and therefore is less affected by self-correlation. Sorbjan (2010a,b) considered three gradient-based scaling systems for the stably stratified boundary layer. Two of them were defined through second-order moments (the temperature variance and the vertical velocity variance) and the potential temperature gradient Γ. The third scaling system does not employ second-order moments, and involves only Γ. The resulting similarity functions are dependent on a single stability parameter, the Richardson number Ri.

A recent analysis of Surface Heat Budget of the Arctic Ocean (SHEBA) data (Sorbjan and Grachev 2010) revealed an additional defect, which is an undesired dependence of bin-averaged similarity functions on height z at which the observations are collected. Such a dependence produces a minor, but noticeable, spread of data points for a given value of the Richardson number. Thus, the primary purpose of our study is to address the described problem and to improve the similarity approach in the stably stratified boundary layer.

The paper has the following structure: the basis of the flux-based and the gradient-based similarity approaches is discussed in Sect. 2, and a new similarity formulation is proposed in Sect. 3. An empirical verification of the improved form of similarity functions is presented in Sect. 4, with final remarks provided in Sect. 5.

2 Similarity Scaling Systems

According to the classic K-theory, the turbulent kinematic fluxes of momentum τ (modulus) and of the potential temperature H, in stably stratified and horizontally homogeneous flow, can be described in terms of the mean wind shear $S = \sqrt{(\mathrm{d}U/\mathrm{d}z)^2 + (\mathrm{d}V/\mathrm{d}z)^2}$ and the potential temperature gradient $\Gamma = \mathrm{d}\Theta/\mathrm{d}z$ (e.g., Sorbjan 2010a,b):

$$\tau = K_m S, \tag{1a}$$

$$H = -K_h \Gamma, \tag{1b}$$

where U and V are components of the wind vector, K_m and K_h are the eddy viscosity and diffusivity, respectively. These can be expressed in the following form:

$$K_m = l_o^2 S f_m(Ri), \tag{2a}$$

$$K_h = l_o^2 S f_h(Ri). \tag{2b}$$

Above, f_m and f_h are empirical functions of the Richardson number $Ri = N^2/S^2$, where $N = \sqrt{\beta\Gamma}$ is the Brunt-Väisälä frequency, $\beta = g/T_o$ is the buoyancy parameter, g is the acceleration due to gravity, T_o is the reference temperature, and $l_o = (\tau^{1/2}/S)_o$ is the mixing length in neutral conditions, defined as a ratio of the momentum flux and shear at $Ri = 0$. In the proximity of the underlying surface, $\tau = u_*^2$, $S = u_*/\kappa z$, which implies that the mixing length is a linear function of height, $l_o = \kappa z$, where k is the von Karman constant. Further from the surface, the growth of the mixing length l_o with height is expected to be less steep than z.

When the empirical functions f_m, f_h and the mixing length l_o are specified, the system (1) and (2) is formally closed, and describes the relationship between the turbulent fluxes τ, H, and parameters S, Γ, β, l_o. Instead of solving such a system of equations, one can employ similarity theory often applied in situations when the complexity of physical processes prevents direct solutions of governing equations being obtained.

The variables appearing in the system (1) and (2) will be used to define local (z-dependent) similarity scales in the stable regime. The choice of the similarity scales for the set of $n = 6$ variables:

$$\{\tau, H, \beta, \Gamma, l_o, S\} \tag{3}$$

with $k = 3$ independent units, [m], [s], [K], is not unique and can be performed in a number of ways. Generally, $n - k = 3$ dimensionally independent parameters in the above list can be selected to build a system of three scales for length, temperature, and velocity. Let us consider two local scaling systems, based on the following choice of parameters:

$$\{\tau, H, \beta\}, \tag{4a}$$

and

$$\{\beta, \Gamma, l_o\}. \tag{4b}$$

The first set of parameters leads to the local "flux-based scaling", while the other set implies the local "gradient-based scaling".

The local flux-based scales first were proposed by Nieuwstadt (1984) as an extension of the surface scales, constant with height, and introduced by Monin and Obukhov (1954):

$$U_*(z) = \tau^{1/2}, \tag{5a}$$

$$\vartheta_*(z) = -\frac{H}{\tau^{1/2}}, \tag{5b}$$

$$\Lambda_*(z) = -\frac{\tau^{3/2}}{\kappa\beta H}. \tag{5c}$$

Employing dimensional analysis, one can conclude that non-dimensional products of a statistical moment X (such as S and Γ, which appear in the list (3), and also other moments, such as e.g., the standard deviations of the vertical velocity σ_w and temperature σ_θ) and the above flux-based scales, are universal functions of a single dimensionless parameter, obtained as a ratio of the mixing length l_o, which is a remaining parameter in the list (3), and the length scale Λ_*:

$$\frac{X}{U_*^a \vartheta_*^b \Lambda_*^c} = \Phi_X\left(l_o/\Lambda_*\right) \tag{6}$$

where the exponents a, b, c are chosen in such a way that the function Φ_X is dimensionless. Specifically, for S and Γ, one obtains:

$$\frac{\Lambda_*}{U_*} S = \Phi_m\left(l_o/\Lambda_*\right), \tag{7a}$$

$$\frac{\Lambda_*}{\vartheta_*} \Gamma = \Phi_h\left(l_o/\Lambda_*\right), \tag{7b}$$

which is equivalent to:

$$\frac{l_o}{U_*} S = \frac{l_o}{\Lambda_*} \Phi_m\left(l_o/\Lambda_*\right) = \Psi_m\left(l_o/\Lambda_*\right), \tag{8a}$$

$$\frac{l_o}{\vartheta_*} \Gamma = \frac{l_o}{\Lambda_*} \Phi_h\left(l_o/\Lambda_*\right) = \Psi_h\left(l_o/\Lambda_*\right). \tag{8b}$$

The expressions (6) and (8) constitute a new and more general form of the flux-based similarity function. For $l_o = \kappa z$, one recovers the local form of similarity functions in the surface layer: $\kappa z S/U_* = \Psi_m\left(z/\Lambda_*\right)$, and $\kappa z \Gamma/\vartheta_* = \Psi_h\left(z/\Lambda_*\right)$.

From Eqs. 8a, b it follows that the local Richardson number Ri is dependent on the dimensionless parameter l_o/Λ_*:

$$Ri \equiv \frac{\beta\Gamma}{S^2} = \frac{l_o}{\kappa\Lambda_*}\frac{\Psi_h\,(l_o/\Lambda_*)}{\Psi_m^2\,(l_o/\Lambda_*)}, \tag{9}$$

and consequently, Eqs. 8a, b can also be rewritten as functions of the Richardson number:

$$\frac{l_o}{U_*}S = \psi_m(Ri), \tag{10a}$$

$$\frac{l_o}{\vartheta_*}\Gamma = \psi_h(Ri). \tag{10b}$$

By using an appropriate form of $l_o(z)$, as a function of height, the validity of the flux-based similarity functions, ψ_m and ψ_h, can be extended to the entire stable boundary layer. This approach, however, is not constructive above the surface layer, because the flux-based scales, U_* and ϑ_*, are generally unknown functions of height.

An alternative similarity scaling can be introduced by using Eq. 4b:

$$U_s = l_o N, \tag{11a}$$

$$T_s = l_o \Gamma, \tag{11b}$$

$$L_s = l_o. \tag{11c}$$

As implied by the dimensional analysis, non-dimensional products of a statistical moment X in the surface layer (such as the fluxes H, τ, and standard deviations, σ_w and σ_θ), and the gradient-based scales (11a–c), are universal functions of the Richardson number Ri:

$$\frac{X}{U_s^a T_s^b L_s^c} = G_X(Ri), \tag{12}$$

where the exponents a, b, c are chosen in such a way that the function G_X is dimensionless.

3 New Similarity Formulation

The similarity formulation (11–12) requires specifying the mixing length l_o. Assuming that in Eqs. 11a–c the dependence of the mixing length on height near the surface is linear, $l_o = \kappa z$, Sorbjan (2010a) proposed the following form of the gradient-based similarity scales valid in the surface layer:

$$U_s = \kappa z N, \tag{13a}$$

$$T_s = \kappa z \Gamma, \tag{13b}$$

$$L_s = \kappa z. \tag{13c}$$

The resulting gradient-based similarity functions for fluxes and standard deviations were obtained based on SHEBA data as the following functions of the Richardson number Ri (in the range $0 < Ri < 0.7$):

$$G_t \equiv \frac{\tau}{U_s^2} = \frac{1}{Ri(1+300Ri^2)^{3/2}}, \tag{14a}$$

$$G_h \equiv -\frac{H}{U_s T_s} = \frac{1}{0.9Ri^{1/2}(1+250Ri^2)^{3/2}}, \tag{14b}$$

$$G_w \equiv \frac{\sigma_w}{U_s} = \frac{1}{0.85Ri^{1/2}(1+450Ri^2)^{1/2}}, \tag{14c}$$

$$G_\theta \equiv \frac{\sigma_\theta}{T_s} = \frac{5}{(1+2500Ri^2)^{1/2}}. \tag{14d}$$

Using Eqs. 14a, b, we can also obtain:

$$\psi_m \equiv \frac{l_o}{U_*} S = \frac{1}{Ri^{1/2} G_t^{1/2}} = (1+300Ri^2)^{3/4}, \tag{15a}$$

$$\psi_h \equiv \frac{l_o}{\vartheta_*} \Gamma = \frac{G_t^{1/2}}{G_h} = 0.9 \frac{(1+250Ri^2)^{3/2}}{(1+300Ri^2)^{3/4}}, \tag{15b}$$

and also:

$$f_m \equiv \frac{K_m}{l_o^2 S} = RiG_t = \frac{1}{(1+300Ri^2)^{3/2}}, \tag{16a}$$

$$f_h \equiv -\frac{K_h}{l_o^2 S} = Ri^{1/2} G_h = \frac{1}{0.9} \frac{1}{(1+250Ri^2)^{3/2}}. \tag{16b}$$

The assumption of linearity for the mixing length (13a)–(13b), (15a)–(15b), and (16a)–(16b) is acceptable only in close proximity to the underlying surface. A closer analysis of SHEBA data reveals that the bin-averaged similarity functions G_t, G_h, G_w, G_θ of the Richardson number Ri do reflect a minor dependence on the height of observations z (Sorbjan 2010a; Sorbjan and Grachev 2010). Such a dependence could be caused by the departure of the mixing length l_o from linearity for greater heights above the surface. It should be mentioned that level 1 at SHEBA was located at 2.2 m above the underlying surface, level 2 at 3.2 m, level 3 at 5.1 m, level 4 at 8.9 m, and level 5 at either 18.2 or 14 m (e.g., Andreas et al. 1999; Persson et al. 2002).

According to Blackadar (1962), the mixing length in the neutral boundary layer is linear near the surface and nearly constant near its top, and can be expressed in the following form:

$$l_o = \frac{\kappa z}{1+\kappa z/\lambda} \tag{17}$$

where λ is an external parameter. Blackadar related λ to two parameters, the geostrophic wind G and the Coriolis parameter f, by assuming that $\lambda = cG/f$, where $c = 2.7 \times 10^{-4}$. Formally, c should be assumed to be dependent on the Rossby number $Ro = G/(fz_o)$, where z_o is the aerodynamic roughness length.

Adopting the Blackadar-type mixing-length formulation, and substituting Eq. 17 into Eq. 11, yields the following gradient-based similarity scales, valid in the surface layer and above:

$$U_s(\lambda) = \frac{\kappa z N}{1+\kappa z/\lambda}, \tag{18a}$$

$$T_s(\lambda) = \frac{\kappa z \Gamma}{1+\kappa z/\lambda}, \tag{18b}$$

$$L_s(\lambda) = \frac{\kappa z}{1+\kappa z/\lambda}. \tag{18c}$$

Note that when $z/\lambda \to 0$, then $U_s(\lambda)$, $T_s(\lambda)$ and $L_s(\lambda)$ coincide with the scales listed in Eq. 13.

For the similarity scales (18), the analogue of (12) is of the form:

$$\frac{X}{U_s^a(\lambda)T_s^b(\lambda)L_s^c(\lambda)} = G_X(Ri). \tag{19}$$

The above expression implies that the dependence of similarity functions G_X on the Richardson number Ri is the same in the surface layer and above. Such a notion will be examined in Sect. 4, based on data collected during the Cooperative Atmospheric-Surface Exchange Study-1999 (CASES-99) experiment.

4 Empirical Verification

The employed set of data (courtesy of Dr. Jielun Sun of the National Center of Atmospheric Research in Boulder, Colorado) contains values of the momentum and heat fluxes, vertical velocity and temperature variances, wind shear S, and temperature gradient Γ, evaluated at nine levels: 0.5, 1.5, 5, 10, 20, 30, 40, 50, and 55 m above the underlying surface, collected during 18 days of the CASES-99 experiment in Kansas, U.S.A., within an interval between 1800 and 0600 LST (e.g., Poulos 2002). The processed fluxes do not contain mesoscale fluctuations, which were removed based on the method of Vickers and Mahrt (2003, 2006). Data affected by airflow distortion due to the anemometer booms at certain wind directions were also eliminated; the block-averaging interval for obtaining mean variables was 10 min. The wind velocity and temperature gradients were estimated using an approach described by Klipp and Mahrt (2004) and Sun (2011).

The plots of the resulting similarity functions G_t, G_h, G_w, G_θ, for fluxes and variances, normalized by the gradient-based scales (13a, b) and (18a, b), are presented in Figs. 1, 2, 3 and 4, and the dimensionless gradients, $\varphi_m = l_o S/U_*$ and $\varphi_h = l_o \Gamma/\vartheta_*$, are depicted in Figs. 5 and 6. The figures show results at two levels, 10 and 50 m above the underlying surface, which were selected as representative of the upper portion of the surface layer, and of the layer above it. Results obtained for the remaining seven levels are similar. In contrast to Sorbjan (2010a), who presented the bin-averaged results, data presented here are not bin-averaged.

Since values of the geostrophic wind G are not available for the employed dataset, Blackadar's scale $l = 2.7 \times 10^{-4} G/f$, could not be applied to evaluate λ, in the definition of scales (18). Instead, the value $\lambda = 12$ m was found as optimal for the employed dataset (i.e., for all nine levels above the surface). For comparison, a similar value of 14.2 m was obtained by Kim and Mahrt (1992), through the use of aircraft data from three different field programs.

A comparison of the dimensionless momentum flux $G_t = \tau/U_s^2$ is depicted in Fig. 1. The values of τ/U_s^2, obtained for $U_s = \kappa z N$ are marked by red circles, while the values obtained for $U_s(\lambda) = \kappa z N/(1 + \kappa z/\lambda)$ are identified by black diamonds, and the stability function (14a) is represented by the blue curve. The data points in Fig. 1a show that the impact of the mixing-length correction at the level of 10 m is relatively small. The red and black data points are generally consistent with the blue curve. Such an impact is significantly larger at the level of 50 m (Fig. 1b), where most of the red circles are located below the blue curve in Fig. 1b, while the black diamonds are grouped around the curve. At $Ri < 0.04$, the data points marked by black diamonds in Fig. 1b, are highly scattered and located below the blue line. This fact is also noticeable in Fig. 5, which displays the dimensionless shear $\varphi_m = Ri^{-1/2} G_t^{-1/2}$.

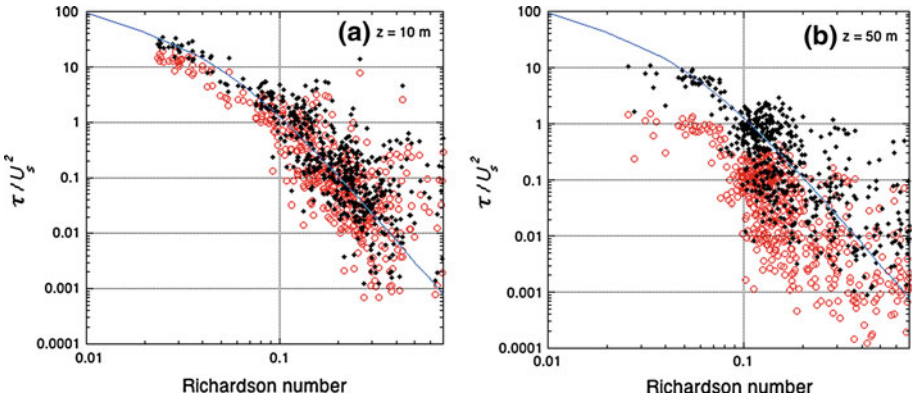

Fig. 1 The dimensionless momentum flux $G_t = \tau/U_s^2$, based on the CASES-99 data at **a** $z = 10$ m, and **b** $z = 50$ m, obtained for $U_s = \kappa z N$ (*red circles*), and for $U_s = \kappa z N/(1 + \kappa z/\lambda)$ with $\lambda = 12$ (*black diamonds*). The stability function of the Richardson number *Ri* (*blue line*), obtained from the SHEBA data, is described by Eq. 14a

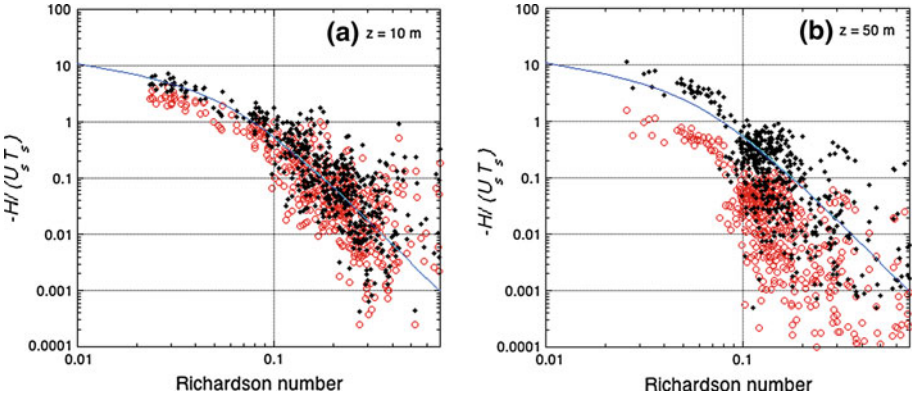

Fig. 2 The dimensionless heat flux $G_h = -H/(U_s T_s)$, based on the CASES-99 data at **a** $z = 10$ m, and **b** $z = 50$ m, obtained for $U_s = \kappa z N$, $T_s = \kappa z \Gamma$ (*red circles*), and for $U_s = \kappa z N/(1+\kappa z/\lambda)$, $T_s = \kappa z \Gamma/(1+\kappa z/\lambda)$ with $\lambda = 12$ (*black diamonds*). The stability function of the Richardson number *Ri* (*blue line*), obtained from the SHEBA data, is described by Eq. 14b

The dimensionless heat flux $G_h = -H/(U_s T_s)$ is shown in Fig. 2, where the same symbols as in Fig. 1 are employed (and also in the remaining Figs. 3, 4, 5 and 6). The values of the dimensionless flux, obtained for U_s and T_s are marked by red circles, and the values evaluated for $U_s(\lambda)$ and $T_s(\lambda)$ are indicated by black diamonds; the stability function (14b) is represented by the blue curve. The figure indicates that the effect of the mixing-length correction at $z = 10$ m is small (Fig. 2a). At the level of 50 m (Fig. 2b), the effect of the mixing-length correction is significant, where most of the red circles are located below the blue curve. On the other hand, the black diamonds are shifted closer to the blue curve (for $Ri > 0.09$). The black diamonds at $Ri < 0.09$, in Fig. 2b, are located slightly above the curve. The influence of this fact can also be seen in Fig. 6, which displays the dimensionless vertical gradient of the potential temperature $\varphi_h = G_t^{1/2} G_h^{-1}$.

Figure 3 shows a comparison of the dimensionless standard deviation of the vertical velocity $G_w = \sigma_w/U_s$, obtained for U_s (red circles) and for $U_s(\lambda)$ (black diamonds); the blue

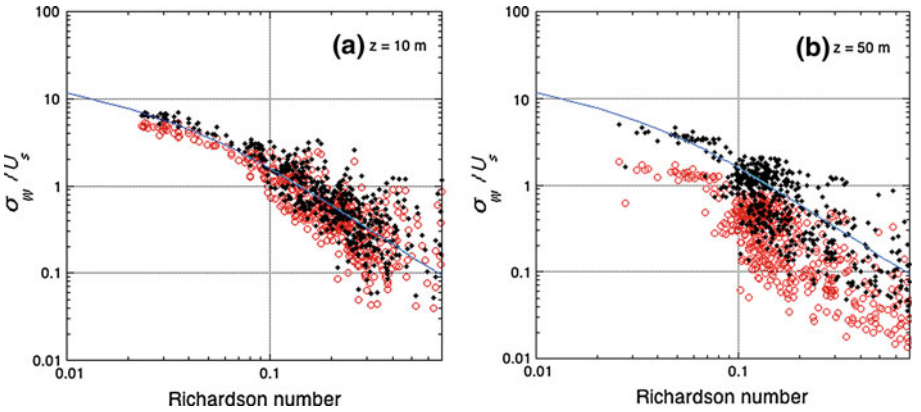

Fig. 3 The dimensionless standard deviation of the vertical velocity $G_w = \sigma_w / U_s$, based on the CASES-99 data at **a** $z = 10$ m, and **b** $z = 50$ m, obtained for $U_s = \kappa z N$ (*red circles*), and for $U_s = \kappa z N / (1 + \kappa z / \lambda)$ with $\lambda = 12$ (*black diamonds*). The stability function of the Richardson number *Ri* (*blue line*), obtained from the SHEBA data, is described by Eq. 14c

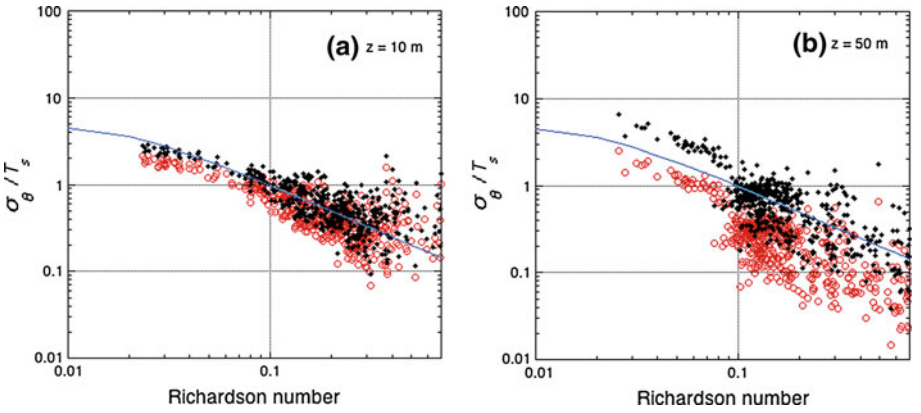

Fig. 4 The dimensionless standard deviation of the potential temperature $G_\theta = \sigma_\theta / T_s$, based on the CASES-99 data at **a** $z = 10$ m, and **b** $z = 50$ m, obtained for $T_s = \kappa z \Gamma$ (*red circles*), and for $T_s = \kappa z \Gamma / (1 + \kappa z / \lambda)$ with $\lambda = 12$ (*black diamonds*). The stability function of the Richardson number *Ri* (*blue line*), obtained from the SHEBA data, is described by Eq. 14d

curve in the figure is described by Eq. 14c. As in Figs. 1 and 2, the result of the mixing-length correction is relatively small at the level of 10 m (Fig. 3a), and larger at the level of 50 m (Fig. 3b). Most of the data points, marked by red circles at $z = 50$ m, are located below the blue curve. The black diamonds are situated closer to the blue curve in the entire range of *Ri*.

The values of the dimensionless standard deviation of the potential temperature $G_\theta = \sigma_\theta / T_s$, obtained for T_s (red circles) and for $T_s(\lambda)$ (black diamonds), are shown in Fig. 4. The effect of the mixing-length correction is minor at the level of 10 m (Fig. 4a), and significant at the level of 50 m in Fig. 4b. Most of the red circles at the level of 50 m in Fig. 4b are located below the blue curve, defined by Eq. 14d, while the black diamonds are placed closer to the curve, especially for larger *Ri*. For $Ri < 0.09$, the black diamonds in Fig. 4b are grouped above the curve.

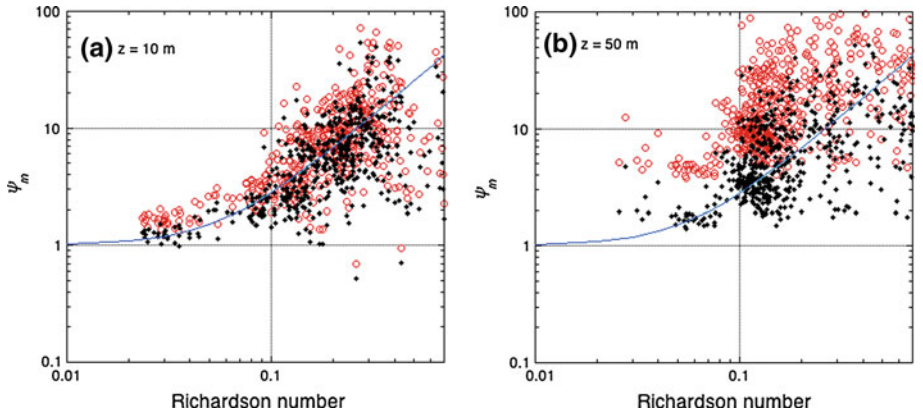

Fig. 5 The dimensionless wind shear $\varphi_m = l_o S/U_* \left(\equiv Ri^{-1/2} G_t^{-1/2}\right)$, based on the CASES-99 data at **a** $z = 10$ m, and **b** $z = 50$ m, obtained for $l_o = \kappa z$ (*red circles*), and for $l_o = \kappa z/(1 + \kappa z/\lambda)$ with $\lambda = 12$ (*black diamonds*). The stability function of the Richardson number *Ri* (*blue line*), obtained from the SHEBA data, is described by Eq. 15a

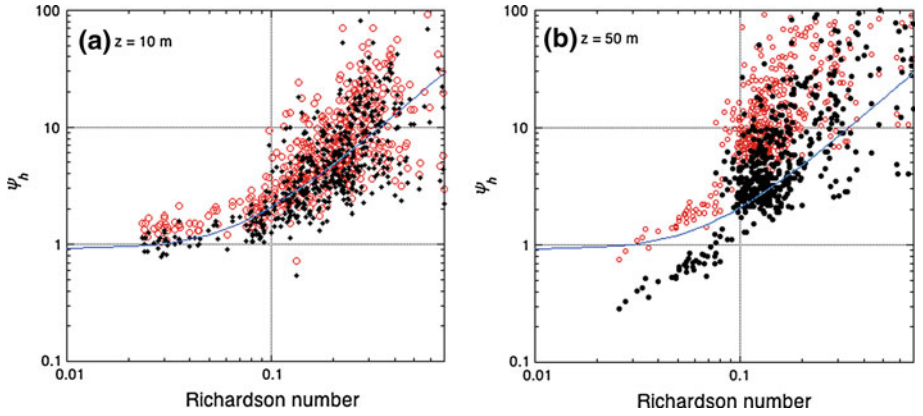

Fig. 6 The dimensionless potential temperature gradient $\varphi_h = l_o \Gamma/\vartheta_* \left(\equiv G_t^{1/2} G_h^{-1}\right)$, based on the CASES-99 data at **a** $z = 10$ m, and **b** $z = 50$ m, obtained for $l_o = \kappa z$ (*red circles*), and for $l_o = \kappa z/(1 + \kappa z/\lambda)$ with $\lambda = 12$ (*black diamonds*). The stability function of the Richardson number *Ri* (*blue line*), obtained from the SHEBA data, is described by Eq. 15b

Figures 5 and 6 show the dimensionless gradients for wind velocity and temperature. The dimensionless values of the wind shear, $\psi_m = l_o S/U_*$, are depicted in Fig. 5, while the dimensionless temperature gradient, $\psi_h = l_o \Gamma/\vartheta_*$, is shown in Fig. 6. The effect of the mixing-length correction at the level of 10 m is minor in Figs. 5a and 6a. Because the function G_t in Fig. 1b lies below the blue curve for small values of *Ri*, consequently, the function $\psi_m = Ri^{-1/2} G_t^{-1/2}$ (black diamonds) in Fig. 5b is located above the blue curve (given by Eq. 15a) for the same range of *Ri*. Similarly, because G_t in Fig. 1b is below the blue curve for small values of Ri, and G_h in Fig. 2b is above the blue curve in-near neutral conditions, consequently the values of the function $\psi_h = G_t^{1/2} G_h^{-1}$ (black diamonds) are located significantly below the blue curve in Fig. 6b, for $Ri < 0.09$.

Figures 1, 2, 3, 4, 5 and 6 imply that the similarity formulation with the Blackadar-type mixing length is supported by the CASES-99 data in stable conditions, for sufficiently large values of Ri. For small values of Ri, the considered moments at $z = 50$ m are inconsistent (with the exception of the standard deviation of the vertical velocity), i.e., either highly scattered (the momentum flux), or overestimated (the heat flux and the temperature standard deviation). This behaviour can be associated with errors in evaluating the Richardson number when the wind velocity and temperature gradients are relatively small.

Equations 15a, b, for the dimensionless gradients ψ_m and ψ_h, together with the non-linear expression for the mixing length (17), formally extend the Monin–Obukhov similarity functions for the entire stable boundary layer. The extension can be practically used to obtain local values of the momentum and temperature fluxes, based on local gradients of the wind velocity components and the potential temperature. The reverse procedure, of obtaining wind and temperature profiles based on fluxes, can be accomplished only in the surface layer, under the assumption that the fluxes are constant with height.

The resulting expressions (16a, b) and (18a, b), for eddy viscosity and diffusivity, K_m and K_h, have been employed as closure assumptions within a single-column model by Sorbjan (2011). Equations 14c, d and 18a, b have been used to diagnose variances of the vertical velocity and temperature. A comparison of the model results (for fluxes and variances) with two high-resolution large-eddy simulation models shows very good agreement, and supports the described above approach.

5 Conclusions

A modified form of gradient-based similarity functions in the stable boundary layer has been proposed and tested using the CASES-99 data. The considered similarity functions are expressed in terms of new gradient-based similarity scales (Eq. 18), which employ the mixing length l_o as a scaling parameter. Blackadar's expression for the mixing length, $l_o = \kappa z/(1 + \kappa z/\lambda)$, has been tested, as opposed to $l_o = \kappa z$, originally proposed by Sorbjan (2010a,b). The value $\lambda = 12$ m is found to best fit the observations obtained during the CASES-99 experiment. The modification of the scales does not alter the dependence of the similarity functions for fluxes and standard deviations on the Richardson number Ri, and is supported by the CASES-99 data in stable conditions (for sufficiently large values of Ri). The introduced modification is also valid for the flux-based similarity functions $\psi_m(Ri)$, and $\psi_h(Ri)$.

The new formulation allows the local values of fluxes and standard deviations for the vertical velocity and temperature to be obtained in the stable boundary layer, based on local gradients of the wind-velocity components and the potential temperature. It can be employed as a closure scheme within single-column models.

Acknowledgments My appreciation is directed to Dr. Jielun Sun (NCAR) for providing the processed CASES-99 data, and to a reviewer for his constructive and helpful comments. The work has been supported by the National Science Foundation grant ATM-0938293.

Open Access This article is distributed under the terms of the Creative Commons Attribution Noncommercial License which permits any noncommercial use, distribution, and reproduction in any medium, provided the original author(s) and source are credited.

References

Andreas EL, Fairall CW, Guest PS, Persson POG (1999) An overview of the SHEBA atmospheric surface flux program. In: Proceedings of the 13th symposium on boundary layers and turbulence. American Meteorological Society, Dallas, TX, pp 550–555

Baas P, Steeneveld GJ, van de Wiel BJH, Holtslag AAM (2006) Exploring self-correlation in flux–gradient relationships for stably stratified conditions. J Atmos Sci 63:3045–3054

Blackadar AK (1962) The vertical distribution of wind and turbulent exchange in neutral atmosphere. J Geophys Res 67:3095–3103

Kim J, Mahrt L (1992) Simple formulation of turbulent mixing in the stable free atmosphere and nocturnal boundary layer. Tellus 44A:381–394

Klipp C, Mahrt L (2004) Flux–gradient relationship, self-correlation and intermittency in the stable boundary layer. Q J Roy Meteorol Soc 130:2087–2104

Monin AS, Obukhov AM (1954) Basic laws of turbulence mixing in the surface layer of the atmosphere. Trudy Geof Inst AN SSSR 24:163–187

Nieuwstadt FTM (1984) The turbulent structure of the stable, nocturnal boundary layer. J Atmos Sci 41: 2202–2216

Persson POG, Fairall CW, Andreas EL, Guest PS, Perovich DK (2002) Measurements near the atmospheric surface flux group tower at SHEBA: near-surface conditions and surface energy budget. J Geophys Res 107(C10):SHE21.1–SHE21.35

Poulos GS et al (2002) Cases99—a comprehensive investigation of the stable nocturnal boundary layer. Bull Am Meteorol Soc 83:555–581

Sorbjan Z (2010a) Scaling and similarity laws in the stable boundary layer. Q J Roy Meteorol Soc 136: 1243–1254

Sorbjan Z (2010b) Recent advances in the similarity theory of the stable boundary layer. In: Zannetti P (ed) Air quality modeling—theories, methodologies, computational techniques, and available databases and software, vol IV, advances and updates. The EnviroComp Institute and the Air & Waste Management Association

Sorbjan Z (2011) A study of the stable boundary layer based on a single-column K-theory model. Boundary-Layer Meteorol. doi:10.1007/s10546-011-9654-9

Sorbjan Z, Grachev AA (2010) An evaluation of the flux–gradient relationship in the stable boundary layer. Boundary-Layer Meteorol 135(3):385–405

Sun J (2011) Vertical variation of mixing length under neutral and stable conditions during CASES99. J Appl Meteorol Clim (in press)

Vickers D, Mahrt L (2003) The cospectral gap and turbulent flux calculations. J Atmos Ocean Technol 20: 660–672

Vickers D, Mahrt L (2006) Solution for flux contamination by mesoscale motions with very weak turbulence. Boundary-Layer Meteorol 118:431–447